arXiv:2405.04293v1 [cond-mat.str-el] 7 May 2024

Observation of Mermin-Wagner behavior in LaFeO$_3$/SrTiO$_3$ superlattices

Michal Kiaba[1*], Andreas Suter[2], Zaher Salman[2], Thomas Prokscha[2], Binbin Chen[3], Gertjan Koster[4] and Adam Dubroka[1,5]

[1*]Department of Condensed Matter Physics, Masaryk University, Kotlářská 2, Brno, 61137, Czech republic.
[2]Laboratory for Muon-Spin Spectroscopy, Paul Scherrer Institute, Villigen, Switzerland.
[3]Key Laboratory of Polar Materials and Devices (MOE) and Department of Electronics, East China Normal University, Shanghai 200241, China.
[4]MESA+ Institute for Nanotechnology, University of Twente, 7500 AE Enschede, The Netherlands.
[5]Central European Institute of Technology, Brno University of Technology, 612 00 Brno, Czech Republic.

*Corresponding author(s). E-mail(s): kiaba@mail.muni.cz;

Abstract

Two-dimensional magnetic materials attract a lot of attention since they potentially exhibit new magnetic properties due to, e.g., strongly enhanced spin fluctuations. However, the suppression of the long-range magnetic order in two dimensions due to long-wavelength spin fluctuations, as suggested by the Mermin-Wagner theorem, has been questioned for finite-size laboratory samples. Here we study the magnetic properties of a dimensional crossover in superlattices composed of the antiferromagnetic LaFeO$_3$ and SrTiO$_3$ that, thanks to their large lateral size, allowed examination using a sensitive magnetic probe — muon spin rotation spectroscopy. We show that the iron electronic moments in superlattices with 3 and 2 monolayers of LaFeO$_3$ exhibit a static antiferromagnetic order. In contrast, in the superlattices with single LaFeO$_3$ monolayer, the moments do not order and fluctuate to the lowest measured temperature as

expected from the Mermin-Wagner theorem. Our work shows how dimensionality can be used to tune the magnetic properties of ultrathin films.

The properties of magnetic films with thickness in the nanoscale have been a long-standing research topic. The theory of critical behavior predicts that the phase transition temperature should decrease with decreasing film thickness [1], which was observed in several cases [2–7]. In the 2-dimensional (2D) limit, Mermin and Wagner [8] extended the initial idea of Hohenberg [9] for a superconductor and predicted complete suppression of the long-range magnetic order in models with continuous rotational symmetries (i.e., with the Heisenberg or XY spin Hamiltonian) at finite temperature due to long-wavelength fluctuations. Importantly, this prediction is strictly valid only for the thermodynamic limit, i.e., for samples with laterally infinite sizes. However, since the divergence of the fluctuations in 2D case is only slow (logarithmic in sample size), it was suggested that for any finite-size laboratory samples, the phase order is preserved for superconductivity [10] and even for magnetism [11].

The discovery of magnetic van der Waals materials allowed the investigation of magnetism in samples with thickness down to a single monolayer [12]. For example, it was reported that in samples of bulk antiferromagnet $NiPS_3$ that are two or more monolayers thick, the magnetic order is preserved, whereas it is suppressed in a single monolayer sample [13]. Since the Hamiltonian of $NiPS_3$ has the XY symmetry, this behavior thus follows the prediction of the Mermin-Wagner theorem rather than the suggestions for preserving the long-range order [11]. However, due to the small lateral size of the single monolayer $NiPS_3$ samples obtained by the exfoliation, the antiferromagnetic order was probed relatively indirectly by Raman spectroscopy via coupling of a phonon to a magnon mode [13].

To test the Mermin-Wagner behavior using a magnetic probe, we study the magnetic properties of three to two-dimensional crossover in superlattices composed of antiferromagnetic $LaFeO_3$ separated by nonmagnetic $SrTiO_3$ layers. Bulk $LaFeO_3$ is a prototypical perovskite antiferromagnetic insulator with Heisenberg symmetry of the spin Hamiltonian [14] and with the highest Neel temperature (T_N) of 740 K among $ReFeO_3$ materials [15], where Re stands for rear earth. It has a high magnetic moment of almost 5 μ_B per Fe^{3+} ion and the G-type structure of the antiferromagnetic state (where each spin is aligned opposite to the nearest neighbor), thus the antiferromagnetic order is expected to be relatively robust. Thanks to the advancement in deposition technology, it is possible to fabricate heterostructures with sharp interfaces that are composed of perovskite oxides with various order parameters, including magnetism,
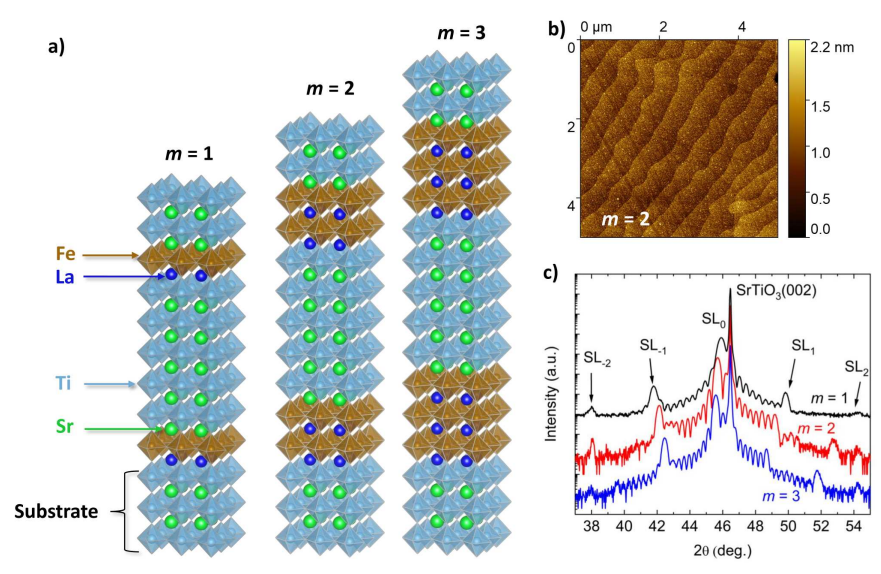
Fig. 1: **Structural characterization of the superlattices.** a) Scheme of $[(LaFeO_3)_m/(SrTiO_3)_5]_{10}$ superlattices near the surface of TiO-terminated $SrTiO_3$ (001) substrate. b) The surface morphology of the $m = 2$ superlattice determined by an atomic force microscope. c) X-ray diffraction spectra exhibiting zero (SL_0), first (SL_1, SL_{-1}) and the second diffraction peaks (SL_2, SL_{-2}) due to the $(LaFeO_3)_m/(SrTiO_3)_5$ bilayer occurring near the (002) diffraction of the $SrTiO_3$ substrate.

ferroelectricity, and superconductivity [16, 17]. Perovskite oxide heterostructures are also promising for applications since they can be used in large-scale samples and devices (see e.g. Refs. [18–21]). Using pulsed laser deposition, we fabricated superlattices with 1, 2, and 3 monolayers of $LaFeO_3$ separated by a non-magnetic spacer of 5 monolayers of $SrTiO_3$ with a large lateral size of 10×10 mm^2 that allowed their investigation using a sensitive magnetic probe — low-energy muon spin rotation spectroscopy [22].

To enhance the signal in the muon spin rotation experiment, we prepared superlattices denoted as $[(LaFeO_3)_m/(SrTiO_3)_5]_{10}$, where a bilayer with $m = 1, 2$ or 3 monolayers of $LaFeO_3$ and five monolayers of $SrTiO_3$ is repeated 10 times. The scheme of the ideal superlattice structure near the interface with the TiO-terminated $SrTiO_3$ (001) substrate is shown in Fig. 1(a). Figure 1(b) displays the surface morphology of the $m = 2$ superlattice measured by an atomic force microscope, which exhibits a flat surface with single unit cell steps copying those of the substrate. The X-ray diffraction spectra, see Fig. 1(c), exhibits zero (SL_0), first (SL_1, SL_{-1}) and the second superlattice diffraction peaks (SL_2, SL_{-2}) due to the $(LaFeO_3)_m/(SrTiO_3)_5$ bilayer, which depict the high structural quality of the superlattices. The thickness of $(LaFeO_3)_m/(SrTiO_3)_5$ bilayer determined from the first order diffraction peak

follows very well the estimates based on the lattice constant of SrTiO$_3$ and LaFeO$_3$, see Supplementary Fig. 1(a).

Investigations of magnetic properties of ultrathin antiferromagnetic layers is a challenging task because of their zero (or very small) average magnetic moment compared to the large total diamagnetic moment of the substrate. To probe the magnetic properties of our superlattices, we have used muon spin rotation spectroscopy, which is sensitive to even very weak local magnetic fields and can distinguish between static and dynamic behavior. We performed the experiments with a low-energy (2 keV) muon beam [22, 23], where spin-polarized muons are implanted into the sample only within about 25 nm deep from the surface, see Supplementary Fig. 1(b). Any magnetic field component transverse to the muon spin direction causes its precession with the Lamour frequency $\omega_L = \gamma_\mu B$, where $\gamma_\mu = ge/2m_\mu$ is the gyromagnetic ratio of the muon and B is the magnitude of the local magnetic field. The time dependence of polarization of the muon spin ensemble (the so-called asymmetry) is measured thanks to the muon decay into a positron preferentially emitted along the muon spin [24].

Zero field muon spin rotation

Figure 2 shows results from the muon spin rotation experiment in zero magnetic field. The time dependence of the muon spin polarization of the superlattices with $m = 3$ and 2, see Figs. 2(a) and 2(b), respectively, exhibit at high temperature a concave Gaussian-like profile and a transition to a faster exponential-like relaxation at lower temperatures. This behavior is consistent with the following qualitative picture: at high temperatures, LaFeO$_3$ layers are in a paramagnetic state where the iron electronic moments are fluctuating too fast to be followed by muons, and thus the depolarization is mainly due to the nuclear moments [25]. With decreasing temperature, the iron electronic moments, that are much larger than the nuclear moments, start ordering, which manifests as a drop of the initial asymmetry and a faster relaxation. In contrast, the asymmetry of the $m = 1$ superlattice shown in Fig. 2(c) is qualitatively different because even at high temperatures, it exhibits a faster depolarization with a convex profile. Such behavior indicates that even at high temperatures, the iron electronic moments fluctuate relatively slowly, which masks the fields due to the nuclear moments.

To get a more quantitative insight, we analyzed the zero field asymmetry, $A_{\mathrm{ZF}}(t)$, with the phenomenological stretched exponential function [26–30]

$$A_{\mathrm{ZF}}(t) = A_0 e^{-(\lambda t)^\beta},\tag{1}$$

where A_0 is the initial asymmetry, λ is the depolarization rate, β is the stretching exponent, and t is time. The parameter β is roughly corresponding to various magnetic states including paramagnetism ($\beta \approx 2$), ordered/disordered magnetism ($\beta \approx 1$) and spin-glass-like states or dynamically fluctuating spin systems ($\beta \approx 0.5$) [26, 31, 32], see Fig. 2(d). The thicker superlattices with
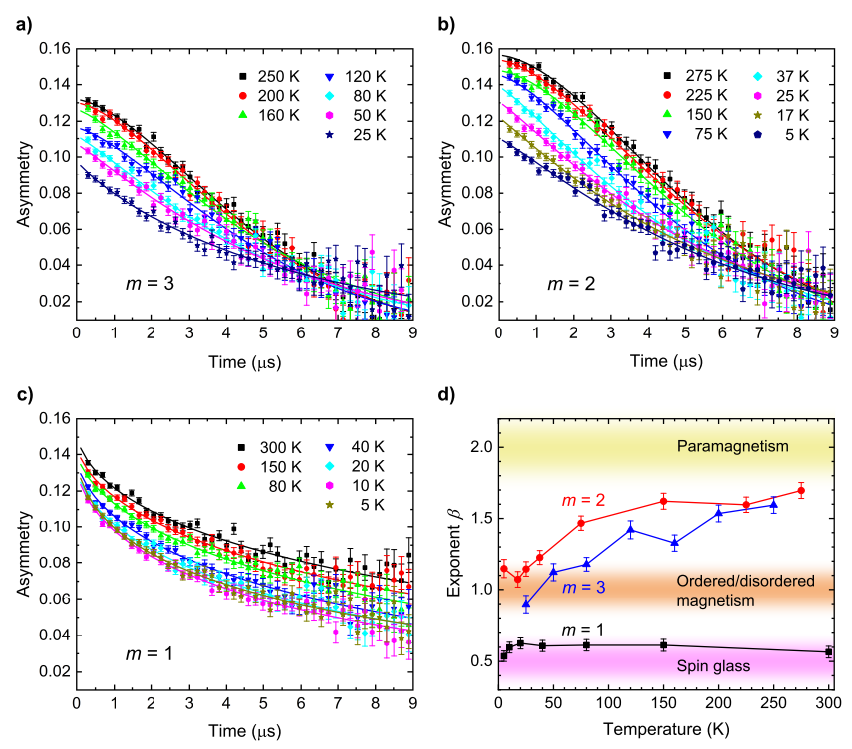
Fig. 2: **Zero field muon spin rotation.** Time evolution of the zero-field muon spin polarisation of $[(LaFeO_3)_m/(SrTiO_3)_5]_{10}$ superlattices with (a) $m = 3$, (b) $m = 2$, and (c) $m = 1$. Error bars represent one standard deviation, and solid lines represent fit by the stretched exponential function (1). (d) Exponent β of the stretched exponential as a function of temperature. Lines represent a guide to the eye. Colored regions show expected values of β for different types of magnetic states.

$m = 2$ and $m = 3$ exhibit expected behavior for an antiferromagnetic phase transition where at high temperatures, the values of β are close to the paramagnetic value of 2, and they decrease towards 1 with decreasing temperature as the static magnetic order sets in. In contrast, for the $m = 1$ superlattice, β is in the whole temperature range close to 0.5. The obtained values of β depict the qualitative difference in the magnetic properties of the $m = 1$ superlattice on the one hand and $m = 2$ and $m = 3$ superlattices on the other hand. A similar qualitative difference can be seen in the values of λ, see Supplementary Fig. 2(b).

The magnetic volume fraction and the Neel temperature

Muon spin rotation spectroscopy offers a way to determine the volume fraction of a magnetically ordered phase using a measurement where a weak external
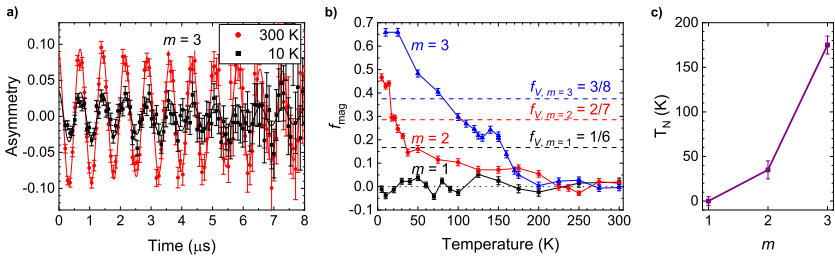
Fig. 3: **The magnetic volume fraction and the Neel temperature**
a) Time evolution of the muon spin polarization in the weak transverse field of
10 mT in the $m = 3$ superlattice at 300 K and 10 K shown with a fit (solid lines)
using Eq. (2). (b) Magnetic volume fraction, f_{mag}, of $[(\text{LaFeO}_3)_m/(\text{SrTiO}_3)_5]_{10}$
superlattices evaluated from the measurement in the weak transverse field.
Horizontal dashed lines represent the volume fraction of LaFeO$_3$ in the super-
lattices. (c) The Neel temperature with respect to m determined from panel
(b).

field is applied transverse to the muon spins. In a paramagnetic state, the
fluctuation rate of electronic moments is too high to influence the muon spin
direction, and thus the muons precess due to the external magnetic field, which
is observed as an oscillation of the asymmetry. Figure 3(a) shows these oscil-
lations in the weak transverse field asymmetry of the $m = 3$ superlattice at
300 K, which is at this temperature in the paramagnetic state. The solid line
represents a fit using the exponentially damped cosine function

$$A_{\text{TF}}(t) = A_0 \, e^{-\lambda_{\text{TF}} t} \cos\left[\gamma_\mu B_{\text{ext}} t + \phi\right] , \qquad (2)$$

where A_0 is the initial asymmetry, λ_{TF} is the depolarisation rate, B_{ext} is the
applied transverse field, and ϕ relates to the initial muon spin polarisation.
In an ordered magnetic phase, muon spins quickly depolarize because of the
large static fields, which leads to the decrease of the oscillation amplitude, as
can be seen in the asymmetry of the $m = 3$ superlattice at 10 K, see Fig. 3(a).
This reduction of the oscillation amplitude is a clear sign of the formation of
a static magnetic order at low temperatures. The magnitude of this decrease
yields the magnetic volume fraction, f_{mag}, which was calculated as

$$f_{\text{mag}}(T) = 1 - \frac{A_0(T)}{A_0(T_{\text{high}})} , \qquad (3)$$

where $A_0(T_{\text{high}})$ is the mean of the initial weak transverse field asymmetry
above 250 K in the expected paramagnetic state. We have determined f_{mag} of
our superlattices using measurements in a transverse field of 10 mT applied
in a perpendicular direction to the superlattice surface. We corrected f_{mag} for
the muonium formation in SrTiO$_3$; for details, see Supplementary Sec. 2.2.

The obtained f_{mag} for the $m = 3$ superlattice, see Fig. 3(b), exhibits an onset near 175 K and increases with lowering the temperature, which is typical for a magnetically ordered state. At 10 K, f_{mag} is above 0.6, which is more than the LaFeO₃ volume fraction, $f_{V,m=3} = 3/8$, which depicts that the antiferromagnetic state is well developed with some stray fields reaching into SrTiO₃ layers. The stray fields are likely caused by the small canting of LaFeO₃ moments [15]. In the $m = 2$ superlattice, $f_{\mathrm{mag}}(T)$ exhibits a weak increase below 200 K, a sharp onset below 35 K and reaches above 0.4 at 5 K. This value is again larger than LaFeO₃ volume fraction $f_{V,m=2} = 2/7$, demonstrating that even in this superlattice with only two monolayers of LaFeO₃, the antiferromagnetic state is well developed at 5 K, although with significantly reduced T_{N} to 35 K. In contrast, f_{mag} of the $m = 1$ superlattice is zero within the experimental error bars down to the lowest measured temperature of 5 K, showing the absence of formation of a static order in the measured temperature range. The qualitative difference between f_{mag} of $m = 3$ and $m = 2$ superlattices on the one hand and of the $m = 1$ superlattice on the other hand again depicts the qualitative difference in their magnetic ground state.

The dependence of T_{N} on m is summarized in Fig. 3(c). Because muons stop in the superlattice at various sites, it is not possible to determine from the data whether the order is ferromagnetic or antiferromagnetic. However, we assume that the observed order is antiferromagnetic since its transition temperature increases with increasing m, and we expect that for large m, the properties should approach those of bulk LaFeO₃. In our superlattices with $m \leq 3$, T_{N} is still much smaller compared to the bulk value of 740 K. To some extent, this reduction can be due to a change of valency of Fe due to proximity to Sr ions at the interface between LaFeO₃ and SrTiO₃. This effect is the strongest in the $m = 1$ superlattice where the iron oxide layer is formed only by one LaO and one FeO₂ layer, see Fig. 1(a), and thus Fe ions are surrounded equally by La and Sr ions. Nevertheless, since bulk La₀.₅Sr₀.₅FeO₃ is still antiferromagnetic with T_{N} of about 250 K [33], we conclude that the strong reduction of T_{N} of $m = 2$ and $m = 1$ superlattices is predominantly due to the dimensional crossover rather than due to the change of the Fe valency.

Differentiation between the static and dynamic magnetism

The zero field and the weak transverse field data indicate that there is no magnetic order in the $m = 1$ superlattice down to 5 K. This could be explained by two scenarios: a static disorder (e.g., due to structural defects) or dynamic fluctuations of the electronic moments. Muon spin rotation spectroscopy offers a way to unequivocally differentiate between static magnetism and dynamically fluctuating fields by measurements in the magnetic field longitudinal to the muon spin direction. In the presence of static magnetism, muons in the longitudinal field with a magnitude much larger than that of the local fields essentially do not precess (so-called decouple from the local fields) and thus do not depolarize in contrast to the zero field measurements. However, if the
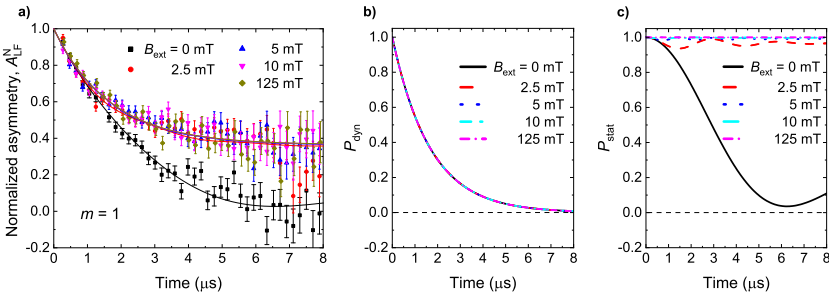
Fig. 4: **Differentiation between the static and dynamic magnetism**
(a) Time evolution of normalized muon spin polarization, A^N_{LF}, of the $m = 1$
superlattice at 5 K for various applied longitudinal magnetic fields. Error bars
represent one standard deviation. The solid lines represent fit using a model
given by Eq. (4). The significant decrease of asymmetry at high fields is a
hallmark of dynamic magnetism. Panels (b) and (c) display the theoretical
Gaussian Kubo-Toyabe functions used in the fit for dynamically fluctuating
moments, P_{dyn}, and for static disordered moments, P_{stat}, respectively.

local fields are fluctuating, they cause a random muon spin-flip (a transition
between the Zeeman split energy levels) and cause the muon-spin depolariza-
tion even in the longitudinal field, essentially the same as in zero field [24].
Time evolutions of muon spin polarization in the $m = 1$ superlattice at 5 K
in several longitudinal fields are shown in Fig. 4(a); data are normalized as
detailed in Supplementary Sec. 2.3. The asymmetry increases between zero
field and 2.5 mT, which is caused by the decoupling of the muon spins from
the static nuclear moments of SrTiO$_3$ [25]. However, for higher fields between
2.5 mT to 125 mT, the asymmetry is essentially field independent and exhibits
at 8 μs considerable depolarization to about 40% of the initial value. Such a
significant depolarization independent of the longitudinal field is a hallmark
of fluctuating electronic moments (see, e.g., Ref. [34]).

    We have modeled the normalized asymmetry in the longitudinal field, A^N_{LF},
as a sum of the theoretical Gaussian Kubo-Toyabe functions for dynamic
fluctuations, P_{dyn} [35] and for the static disorder, P_{stat} [25]

$$A^N_{\mathrm{LF}} = c\,P_{\mathrm{dyn}} + (1 - c)\,P_{\mathrm{stat}} , \qquad (4)$$

where c is the volume fraction of the fluctuating part; for details see Supple-
mentary Sec. 2.3. The global fit for all longitudinal fields B_{ext}, see solid lines
in Fig. 4(a), yields the volume fraction $c = 0.64 \pm 0.06$ and the distribution
of the static disordered moments $\sigma_{\mathrm{s}}/\gamma_\mu = 0.32 \pm 0.08$ mT. The functions P_{dyn}
displayed in Fig. 4(b) for the obtained parameter values are essentially field
independent and vanish at 8 μs. In contrast, P_{stat}, displayed in Fig. 4(c), sensi-
tively depends on the external magnetic field. This difference allows the model
to discern between static disorder and dynamically fluctuating moments. The
obtained value of $\sigma_{\mathrm{s}}/\gamma_\mu = 0.32 \pm 0.08$ mT is typical for nuclear moments [25].

It corresponds to regions in SrTiO$_3$ where the dipolar fields from the iron moments are smaller compared to the nuclear fields. This area's volume fraction of $(1-c) = 0.36$ corresponds to the width of about 2.2 monolayers, presumably located in the middle of SrTiO$_3$ layers. The fact that we can fit the data with the model yielding such a small value of σ_s/γ_μ at all external fields is incompatible with the picture of statically disordered iron moments with local fields expected to be in the order of 100-250 mT [36]. If iron moments were static, the increase of the longitudinal field between 10 and 125 mT would lead to a significant increase in the asymmetry [24]. The field-independent asymmetry exhibiting such a considerable depolarization for fields above 2.5 mT can be explained only as a consequence of the fluctuating iron moments.

In summary, the muon spin rotation data in zero, transverse and longitudinal fields consistently show that (i) $m = 3$ and $m = 2$ superlattices exhibit a long-range antiferromagnetic order with T_N of 175 K and 35 K, respectively, (ii) that the magnetic properties of the $m = 1$ superlattice are qualitatively different with no long-range order down to the lowest measured temperature of 5 K and (iii) that at this temperature, the electronic moments are fluctuating rather than statically disordered. These findings point towards a dimensional magnetic crossover where for the superlattice with a single monolayer of iron oxide, the static antiferromagnetic order is lost due to enhanced magnitude of spin fluctuations, as expected from the Mermin-Wagner theorem.

References

[1] Fisher, M. E. & Barber, M. N. Scaling theory for finite-size effects in the critical region. *Phys. Rev. Lett.* **28**, 1516–1519 (1972). https://doi.org/10.1103/PhysRevLett.28.1516

[2] Schneider, C. M. et al. Curie temperature of ultrathin films of fcc-cobalt epitaxially grown on atomically flat Cu(100) surfaces. *Phys. Rev. Lett.* **64**, 1059–1062 (1990). https://doi.org/10.1103/PhysRevLett.64.1059

[3] Fullerton, E. E., Riggs, K. T. Sowers, C. H., Bader, S. D. & Berger, A., Suppression of biquadratic coupling in Fe/Cr(001) superlattices below the Néel transition of Cr. *Phys. Rev. Lett.* **75**, 330–333 (1995). https://doi.org/10.1103/PhysRevLett.75.330

[4] Ambrose, T. & Chien, C. L. Finite-size effects and uncompensated magnetization in thin antiferromagnetic CoO layers. *Phys. Rev. Lett.* **76**, 1743–1746 (1996). https://doi.org/10.1103/PhysRevLett.76.1743

[5] Abarra, E. N., Takano, K., Hellman, F. & Berkowitz, A. E. Thermodynamic measurements of magnetic ordering in antiferromagnetic superlattices. *Phys. Rev. Lett.* **77**, 3451–3454 (1996). https://doi.org/10.1103/PhysRevLett.77.3451

[6] Zhang, R. & Willis, R. F. Thickness-dependent curie temperatures of ultrathin magnetic films: Effect of the range of spin-spin interactions. *Phys. Rev. Lett.* **86**, 2665–2668 (2001). https://doi.org/10.1103/PhysRevLett.86.2665

[7] Lang, X. Y., Zheng, W. T. & Jiang, Q. Size and interface effects on ferromagnetic and antiferromagnetic transition temperatures. *Phys. Rev. B* **73**, 224444 (2006). https://doi.org/10.1103/PhysRevB.73.224444

[8] Mermin, N. D. & Wagner, H. Absence of ferromagnetism or antiferromagnetism in one- or two-dimensional isotropic heisenberg models. *Phys. Rev. Lett.* **17**, 1133–1136 (1966). https://doi.org/10.1103/PhysRevLett.17.1133

[9] Hohenberg, P. C. Existence of long-range order in one and two dimensions. *Phys. Rev.* **158**, 383–386 (1967). https://doi.org/10.1103/PhysRev.158.383

[10] Palle, G. & Sunko, D. K. Physical limitations of the Hohenberg–Mermin–Wagner theorem. *J. Phys. A Math. Theor.* **54**, 315001 (2021). https://doi.org/10.1088/1751-8121/ac0a9d

[11] Jenkins, S. et al. Breaking through the Mermin–Wagner limit in 2D Van der Waals magnets. *Nat. Commun.* **13**, 6917 (2022). https://doi.org/10.1038/s41467-022-34389-0

[12] Burch, K. S., Mandrus, D. & Park, J.-G. Magnetism in two-dimensional Van der Waals materials. *Nature* **563**, 47–52 (2018). https://doi.org/10.1038/s41586-018-0631-z

[13] Kim, K. et al. Suppression of magnetic ordering in XXZ-type antiferromagnetic monolayer NiPS$_3$. *Nat. Commun.* **10**, 345 (2019). https://doi.org/10.1038/s41467-018-08284-6

[14] McQueeney, R. J., Yan, J.-Q., Chang, S. & Ma, J. Determination of the exchange anisotropy in perovskite antiferromagnets using powder inelastic neutron scattering. *Phys. Rev. B* **78**, 184417 (2008). https://doi.org/10.1103/PhysRevB.78.184417

[15] Eibschütz, M., Shtrikman, S. & Treves, D. Mössbauer studies of Fe^{57} in orthoferrites. *Phys. Rev.* **156**, 562–577 (1967). https://doi.org/10.1103/PhysRev.156.562

[16] Hwang, H. Y. et al. Emergent phenomena at oxide interfaces. *Nat. Mater.* **11**, 103–113 (2012). https://doi.org/10.1038/nmat3223

[17] Chen, H. & Millis, A. Charge transfer driven emergent phenomena in oxide heterostructures. *J. Phys. Condens. Matter* **29**, 243001 (2017). https://doi.org/10.1088/1361-648X/aa6efe

[18] Ueno, K. et al. Electric-field-induced superconductivity in an insulator. *Nat. Mater.* **7**, 855–858 (2008). https://doi.org/10.1038/nmat2298

[19] Bell, C. et al. Dominant mobility modulation by the electric field effect at the LaAlO$_3$/SrTiO$_3$ interface. *Phys. Rev. Lett.* **103**, 226802 (2009). https://doi.org/10.1103/PhysRevLett.103.226802

[20] Kozuka, Y. et al. Insulating phase of a two-dimensional electron gas in Mg$_x$Zn$_{1-x}$O/ZnO heterostructures below ν=13. *Phys. Rev. B* **84**, 033304 (2011). https://doi.org/10.1103/PhysRevB.84.033304

[21] Rong, Y. et al. Challenges for commercializing perovskite solar cells. *Science* **361** (2018). https://doi.org/10.1126/science.aat8235

[22] Prokscha, T. et al. The new μE4 beam at PSI: A hybrid-type large acceptance channel for the generation of a high intensity surface-muon beam. *Nucl. Instrum. Methods Phys. Res. A: Accel. Spectrom. Detect. Assoc. Equip.* **595**, 317–331 (2008). https://doi.org/10.1016/j.nima.2008.07.081

[23] Suter, A., Martins, M. M., Ni, X., Prokscha, T. & Salman, Z. Low energy measurements in Low-Energy μSR. *J. Phys.: Conf. Ser.* **2462**, 012011 (2023). https://doi.org/10.1088/1742-6596/2462/1/012011

[24] Blundell, S. J. Spin-polarized muons in condensed matter physics. *Contemp. Phys.* **40**, 175–192 (1999). https://doi.org/10.1080/001075199181521

[25] Hayano, R. S. et al. Zero-and low-field spin relaxation studied by positive muons. *Phys. Rev. B* **20**, 850–859 (1979). https://doi.org/10.1103/PhysRevB.20.850

[26] Fowlie, J. et al. Intrinsic magnetism in superconducting infinite-layer nickelates. *Nat. Phys.* **18**, 1043–1047 (2022). https://doi.org/10.1038/s41567-022-01684-y

[27] Cantarino, M. R. et al. Dynamic magnetism in the disordered hexagonal double perovskite BaTi$_{1/2}$Mn$_{1/2}$O$_3$. *Phys. Rev. B* **99** (2019). https://doi.org/10.1103/PhysRevB.99.054412

[28] Mustonen, O. et al. Spin-liquid-like state in a spin-1/2 square-lattice antiferromagnet perovskite induced by d^{10}-d^0 cation mixing. *Nat. Commun.* **9** (2018). https://doi.org/10.1038/s41467-018-03435-1

[29] Bert, F. et al. Direct evidence for a dynamical ground state in the highly frustrated Tb$_2$Sn$_2$O$_7$ pyrochlore. *Phys. Rev. Lett.* **97** (2006). https://doi.org/10.1103/PhysRevLett.97.117203

[30] Keren, A. et al. Magnetic dilution in the geometrically frustrated SrCr$_{9p}$Ga$_{12-9p}$O$_{19}$ and the role of local dynamics: A muon spin relaxation study *Phys. Rev. Lett.* **84**, 3450–3453 (2000). https://doi.org/10.1103/PhysRevLett.84.3450

[31] Uemura, Y. J. et al. Spin fluctuations in frustrated kagomé lattice system SrCr$_8$Ga$_4$O$_{19}$ studied by muon spin relaxation. *Phys. Rev. Lett.* **73**, 3306–3309 (1994). https://doi.org/10.1103/PhysRevLett.73.3306

[32] Cho, H. et al. Dynamic spin fluctuations in the frustrated *A*-site spinel CuAl$_2$O$_4$. *Phys. Rev. B* **102**, 014439 (2020). https://doi.org/10.1103/PhysRevB.102.014439

[33] Matsuno, J. et al. Photoemission and hartree-fock studies of oxygen-hole ordering in charge-disproportionated La$_{1-x}$Sr$_x$FeO$_3$. *Phys. Rev. B* **60**, 4605–4608 (1999). https://doi.org/10.1103/PhysRevB.60.4605

[34] Balz, C. et al. Physical realization of a quantum spin liquid based on a complex frustration mechanism. *Nat. Phys.* **12**, 942–949 (2016). https://doi.org/10.1038/nphys3826

[35] Keren, A. Generalization of the abragam relaxation function to a longitudinal field. *Phys. Rev. B* **50**, 10039–10042 (1994). https://doi.org/10.1103/PhysRevB.50.10039

[36] Holzschuh, E., Denison, A. B., Kündig, W., Meier, P. F. & Patterson, B. D. Muon-spin-rotation experiments in orthoferrites. *Phys. Rev. B* **27**, 5294–5307 (1983). https://doi.org/10.1103/PhysRevB.27.5294

[37] Nečas, D. & Klapetek, P. Gwyddion: an open-source software for spm data analysis. *Open Phys.* **10**, 181–188 (2012). https://doi.org/10.2478/s11534-011-0096-2

[38] Momma, K. & Izumi, F. Vesta 3 for three-dimensional visualization of crystal, volumetric and morphology data. *J. Appl. Crystallogr.* **44**, 1272–1276 (2011). https://doi.org/10.1107/S0021889811038970

[39] Suter, A. & Wojek, B. M. Musrfit: A free platform-independent framework for μsr data analysis. *Phys. Procedia* **30**, 69–73 (2012). https://doi.org/10.1016/j.phpro.2012.04.042

Methods

Sample growth and characterization

Superlattices were fabricated by pulsed laser deposition on 10×10 mm^2 TiO-terminated SrTiO$_3$ (001) substrates. The deposition temperature of the substrates was 570 °C, and the background oxygen pressure was 0.01 mbar. The thickness of layers was *in situ* controlled by reflection of high-energy electron diffraction. The samples were annealed *ex situ* in an oxygen atmosphere at 550 °C to reduce the concentration of oxygen vacancies. We fabricated sets of 3-4 samples of each superlattice that formed a sample mosaic to improve the signal-to-noise ratio of the muon spin rotation data. The structural quality of the superlattices was characterized using an atomic force microscope (Bruker Dimension Icon) and X-ray diffractometer (Rigaku Smartlab). Atomic force microscope images were analyzed by Gwyddion software [37] and the superlattice structure shown in Fig. 1(a) by VESTA software [38].

Low-energy muon spin rotation

Low-energy muon spin rotation experiments were performed at the μE4 beamline of the Swiss Muon Source at Paul Scherrer Institute, Villigen. We have used 2 keV muon beam that results in an implantation profile, where most of the muons stop in the superlattices, see Supplementary Fig. 1(b). μSR data were analyzed using musrfit [39].

Acknowledgements

Supplementary online material
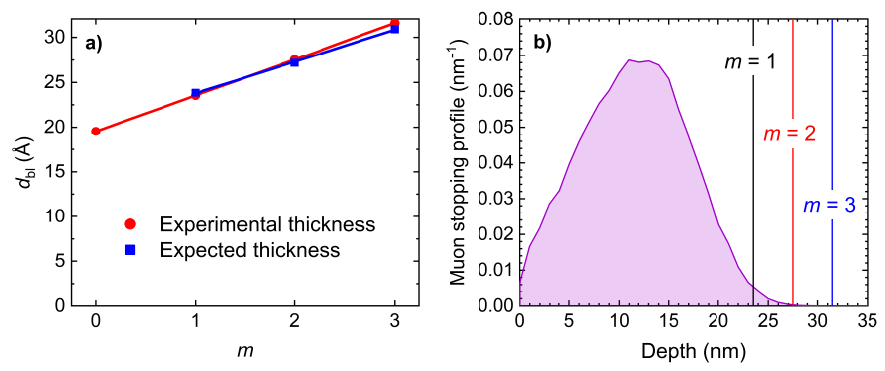
1 Sample characterization

The X-ray diffraction data shown in Fig. 1(c) exhibit the superlattice diffraction peaks (SL_{-1} and SL_1) of the $(LaFeO_3)_m+(SrTiO_3)_5$ bilayer. The thickness of the bilayer was determined from the angular position of these diffraction peaks using the Bragg equation. Supplementary Fig. 1(a) shows the obtained bilayer thickness as a function of m, which is in good agreement with the thickness expected from the bulk lattice constants of $SrTiO_3$, $a_{SrTiO_3} = 3.905$ Å, and out-of-plane pseudo-cubic lattice constant of epitaxial $LaFeO_3$ film, $a_{LaFeO_3} = 4.009$ Å.

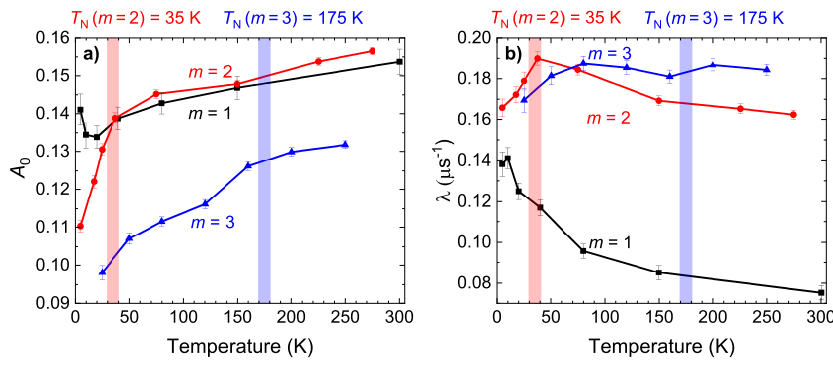## 2 Low energy muon spin rotation

The low-energy muon spin rotation ($LE\mu SR$) spectroscopy [1, 2] with relatively small muon penetration depth compared to the standard muon spin rotation (μSR) enables studying thin films and heterostructures. We have used the muon beam with 2 keV that provides an implantation profile where most of the muons stop in the superlattices; see Supplementary Fig. 1(b). The implantation profile was calculated using Monte Carlo TRIM.SP code [3]. Data in all measurements are analyzed above 0.1 μs since below, strong systematic error due to back reflection of muons arise [2].

2.1 Zero field muon spin rotation

The zero-field asymmetry spectra presented in Fig. 2(a)-(c) do not exhibit any oscillatory time evolution typically seen in bulk crystals. This arises because

Supplementary Fig. 1: (a) Comparison of the thickness of $(LaFeO_3)_m+(SrTiO_3)_5$ bilayer, d_{bl}, determined from X-ray diffraction and the one expected from $SrTiO_3$ and $LaFeO_3$ lattice constants as detailed in the text. (b) Simulated implantation profile for a muon beam energy of 2 keV. Vertical lines mark the thicknesses of $[(LaFeO_3)_m/(SrTiO_3)_5]_{10}$ superlattices.
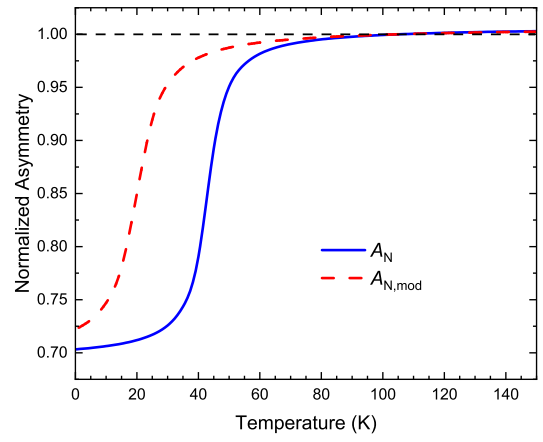
Supplementary Fig. 2: (a) Initial asymmetry, A_0, and (b) depolarization rate, λ, obtained from the fit of zero field data using Eq. (1). The highlighted areas mark Neel temperature of $m = 2$ and $m = 3$ superlattices.

the structure of our superlattices leads to a broad distribution of internal fields, including the stray fields due to the iron spin canting that spread through SrTiO$_3$ layers. This corresponds to a large distribution of Larmor frequencies inevitably leading to a fast damping of the oscillations.

The time evolution of the zero-field asymmetry presented in Fig. 2(a)-(c) was fitted using the stretched exponential function (1) whose exponent β is shown in Fig. 2(d). For completeness, values of the other fitted parameters, i.e., the initial asymmetry, A_0, and the depolarization rate, λ, are shown in Supplementary Figs. 2(a) and 2(b), respectively. The temperature dependence of A_0 exhibits a noticeable decrease below T_N, that is, below 175 K for the $m = 3$ and below 35 K for the $m = 2$ superlattice. This decrease is expected in an ordered magnetic phase where the muons quickly depolarize due to strong static local fields. In the $m = 1$ superlattice, A_0 exhibits only a gradual and relatively weak decrease with decreasing temperature without a sharper onset in agreement with the interpretation that there is no static order in this super-lattice. Surprisingly, A_0 of the $m = 1$ superlattice seems to increase from 10 to 5 K. However, this increase is on the level of one standard deviation, and we do not consider it significant enough.

The temperature dependence of λ, shown in Supplementary Fig. 2(b), is roughly constant for $m = 3$ and $m = 2$ superlattices with values of λ in the range from 0.16 to 0.19 μs^{-1}. It exhibits only a small indication of a decrease with decreasing temperature below T_N, particularly in the $m = 2$ superlattice, connected with the formation of the static magnetic order. In contrast, in the $m = 1$ superlattice, the values of λ are above 100 K about two times smaller compared to $m = 3$ and $m = 2$ superlattices. In addition, λ significantly increases with decreasing temperature below 100 K to about 0.14 μs^{-1} at 5 K compared to 0.075 μs^{-1} at 300 K. This almost doubling of the depolarization rate with decreasing temperature is a strong indication of a decrease in the electronic fluctuation rate. The latter is a typical signature

Supplementary Fig. 3: Normalized asymmetry due to the muonium formation in SrTiO$_3$ expressed by Eq. (5) (blue solid line) and Eq. (7) (red dashed line).
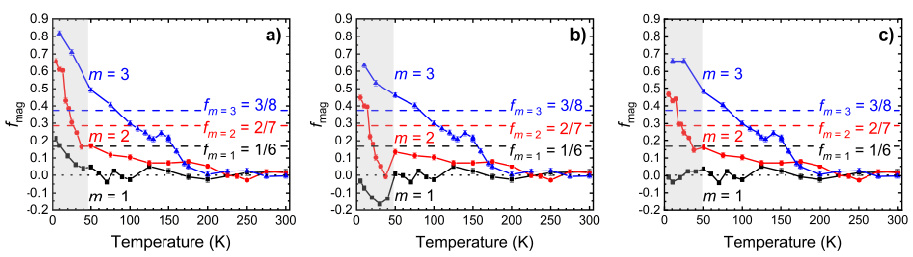
of a fluctuating magnetic ground state [4]. The qualitative and quantitative difference of the temperature dependence of λ between $m = 3$ and $m = 2$ superlattices on the one hand and the $m = 1$ superlattice on the other hand again depicts the difference in their respective magnetic ground states. Note that in the case of the $m = 2$ superlattice, the temperature dependence of λ exhibits a clear maximum at T_{N} of about 35 K with a significant decrease below. This behavior is expected for a static magnetic order that sets in at a phase transition temperature [5].

2.2 Weak transverse field muon spin rotation

In the weak transverse field data analysis, we shall consider the formation of muonium (a bound state of a muon and an electron) in SrTiO$_3$. Because the muon spin in muonium precesses at a different frequency than a free muon spin, the formation of muonium occurring below about 50 K in SrTiO$_3$ [6] influences the weak transverse field data of our superlattices. The temperature dependence of the normalized weak transverse field asymmetry for SrTiO$_3$ at 1.6 keV implanting energy was described by the empiric equation [6]

$$A_{\mathrm{N}}(T) = 0.1 \arctan \frac{T - 43}{4.427} + 0.85 \, , \tag{5}$$

see Supplementary Fig. 3. Our measurements were performed at the implanting muon energy of 2 keV, which is close enough to use Eq. (5) as a starting point in muonium correction. Assuming that the muonium is formed only in SrTiO$_3$ layers, the depolarization due to the muonium formation is subtracted from

Supplementary Fig. 4: Magnetic volume fractions obtained from the weak transverse field measurement. Panel (a) shows values obtained without the correction for muonium formation, and panels (b) and (c) show those corrected for the muonium formation using Eq. (5) and Eq. (7), respectively.

the data using the following equation

$$A_{0,c}(T) = A_0(T) + f_{\text{SrTiO}_3} \left[1 - A_{\text{N}}(T)\right] A_0(T_{\text{high}}) , \tag{6}$$

where f_{SrTiO_3} is the volume fraction of SrTiO_3 in a given superlattice, and $A_0(T_{\text{high}})$ is the asymmetry at high enough temperature. For $A_0(T_{\text{high}})$ we have used a mean value above 250 K where the superlattices are in the paramagnetic state and the influence of muonium is negligible. The correction for the muonium formation is significant only below the temperature of the muonium formation of about 50 K, where $A_{\text{N}}(T)$ is significantly smaller than unity, see Supplementary Fig. 3. At higher temperatures, $A_{\text{N}}(T) \approx 1$ and the second term on the right-hand side of Eq. (6) vanishes.

The magnetic volume fraction of the superlattice, $f_{\text{mag}}(T)$, is calculated as [7]

$$f_{\text{mag}}(T) = 1 - \frac{A_{0,c}(T)}{A_{0,c}(T_{\text{high}})} , \tag{7}$$

where $A_{0,c}(T_{\text{high}})$ is the mean of the initial weak transverse field asymmetry above 250 K in the expected paramagnetic state. Supplementary Fig. 4(a) shows f_{mag} calculated without the muonium correction (using $A_{\text{N}}(T) = 1$). The shaded regions show temperatures below about 50 K where the muonium formation takes place. Values of f_{mag} corrected for the muonium formation using Eq. (5), see Supplementary Fig. 4(b), suddenly decrease below about 50 K for superlattices with $m = 2$ and $m = 1$, which leads, for the case of $m = 1$, even to nonphysical values significantly below zero. Most likely, the step-like correction for muonium formation using Eq. (5), which was obtained on SrTiO_3 single crystal, is sharper and centered at a different temperature than what would be appropriate for ultrathin SrTiO_3 layers of our superlattices. We have therefore adjusted the temperature and width of the transition in Eq. (5) where the muonium formation occurs so that f_{mag} is not negative for

the superlattice $m = 1$. This approach yielded

$$A_{N,\text{mod}}(T) = 0.1 \arctan \frac{T - 20}{6} + 0.85 \, , \tag{8}$$

see Supplementary Fig. 3(b). Corresponding f_{mag} is shown in Supplementary Fig. 4(c) and in the main part of the paper in Fig. 3(b). Note that we did not adjust the multiplication factor of the step-like arctan function in Eq. (8) corresponding to the magnitude of the correction. Consequently, the values of f_{mag} at 5 K resulting from the two corrections [cf. Supplementary Figs. 4(b) and 4(c)] are almost the same. Similarly, the main conclusions are the same: the magnetic volume fraction in the $m = 1$ superlattice at 5 K is essentially zero corresponding to the absence of a static order formed in the measured temperature range in contrast to the $m = 2$ superlattice where it is significantly above zero (above 0.4 and above $LaFeO_3$ volume fraction of $2/7$) and thus the superlattice exhibits a static antiferromagnetic order.

2.3 Longitudinal field muon spin rotation

Supplementary Fig. 5 shows the asymmetry of the $m = 1$ superlattice measured at 5 K for several longitudinal fields. The data are analyzed with the model

$$A_{\text{LF}}(t, B_{\text{ext}}) = A\left[c\,P_{\text{dyn}}(t, B_{\text{ext}}) + (1 - c)P_{\text{stat}}(t, B_{\text{ext}})\right] + A_0(B_{\text{ext}}) \, . \tag{9}$$

Here $A_0(B_{\text{ext}})$ is a background asymmetry which, in principle, depends on magnetic field B_{ext}. In LEμSR, muons are focused onto the sample by the external magnetic field, and thus different magnetic fields give rise to a different background. A is the normalization constant that is field independent. The depolarization due to the sample is modeled as a weighted average of the theoretical Gaussian Kubo-Toyabe functions for the static disorder, P_{stat} [8],
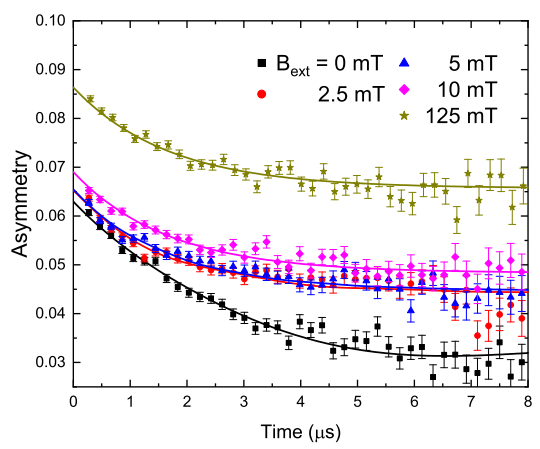
$$P_{\text{stat}}(B_{\text{ext}} = 0, t) = \frac{1}{3} + \frac{2}{3}(1 - \sigma_s^2 t^2) \exp\left[-\frac{\sigma_s^2 t^2}{2}\right] \, , \tag{10}$$

$$\begin{aligned} P_{\text{stat}}(B_{\text{ext}}, t) = 1 - \frac{2\sigma_s^2}{(\gamma_\mu B_{\text{ext}})^2}\left[1 - \exp\left(-\frac{\sigma_s^2 t^2}{2}\right)\cos\left(\gamma_\mu B_{\text{ext}} t\right)\right] + \\ + \frac{2\sigma_s^4}{(\gamma_\mu B_{\text{ext}})^3}\int_0^t \exp\left(\frac{\sigma_s^2 \tau^2}{2}\right)\sin\left(\gamma_\mu B_{\text{ext}}\tau\right)d\tau \, , \end{aligned} \tag{11}$$

and the dynamic fluctuation, P_{dyn} [9],

$$P_{\text{dyn}}(B_{\text{ext}}, t) = \exp\left[-\frac{2\sigma_d^2 \nu}{(\gamma_\mu B_{\text{ext}})^2 + \nu^2}t\right] \, , \tag{12}$$

where ν is the fluctuation rate. The depolarization rate σ appearing in Eqs. (10)-(12) is defined as $\sigma = \gamma_\mu\sqrt{<\Delta B^2>}$ where $<\Delta B^2>$ is the second

Supplementary Fig. 5: Time evolution of the asymmetry from longitudinal field measurement of the $m = 1$ superlattice at 5 K for several applied magnetic fields displayed together with a model (solid lines), see Eq. (9). The error bars denote one standard deviation.

Variable	Value
σ_s/γ_μ [mT]	0.32 ± 0.08
σ_d/γ_μ [mT] fixed	250
ν [GHz]	150 ± 20
c	0.64 ± 0.06
A	0.032 ± 0.003
$A_0(B_{ext} = 0$ mT$)$	0.030 ± 0.002
$A_0(B_{ext} = 2.5$ mT$)$	0.032 ± 0.003
$A_0(B_{ext} = 5$ mT$)$	0.032 ± 0.003
$A_0(B_{ext} = 10$ mT$)$	0.036 ± 0.003
$A_0(B_{ext} = 125$ mT$)$	0.053 ± 0.003

Table 1: Values of parameters obtained from the global fit of the longitudinal field data by Eq. (9). The errors represent one standard deviation.

moment of the field distribution. The subscripts 's' and 'd' denote whether the second moment corresponds to the static or dynamic magnetic field distribution. The volume fraction of the dynamically fluctuating part is expressed by the field-independent parameter c.

The data shown in Supplementary Fig. 5 (points) were analyzed with a global fit of asymmetries at all measured fields with the model expressed by Eq. (9) (solid lines). The obtained values of parameters are shown in Tab. 1. Because of the high correlation between σ_{dyn} and the fluctuation rate ν, we fixed the distribution width of the dynamically fluctuating moments, σ_{dyn}/γ_μ, to 250 mT since similar values of the internal fields were observed in orthoferrites [10]. The corresponding value of the fluctuation rate is $\nu = 150 \pm 20$ GHz. The obtained value $\sigma_s/\gamma_\mu = 0.32 \pm 0.08$ mT exhibits a relatively large error

that is due to the comparably large field of 2.5 mT used in the measurements. To determine this value with better precision, one would need to measure with significantly smaller fields. The errors of other values shown in Tab. 1 are reasonably low (about 10%), which demonstrates that the global fit is well conditioned. Particularly, the fit allowed us to determine the constants A and $A_0(B_{\text{ext}})$ with reasonable precision. For the sake of simplicity, we display in Fig. 4 the data as normalized asymmetry

$$A_{\text{LF}}^N(t, B_{\text{ext}}) = [A_{\text{LF}}(t, B_{\text{ext}}) - A_0(B_{\text{ext}})]/A \ . \tag{13}$$

3 Run logs

Measurement	T [K]	E [keV]	B [mT]	run no.	year
Zero field	300	1.96	0	4664	2022
	150	1.96	0	4693	2022
	80	1.96	0	4665	2022
	40	1.96	0	4666	2022
	20	1.96	0	4667	2022
	10	1.96	0	4668	2022
	5	1.96	0	4669	2022
Weak transverse field	300	2.01	10	6608	2021
	250	2.01	10	6609	2021
	200	2.01	10	6610	2021
	175	2.01	10	6611	2021
	150	2.01	10	6612	2021
	125	2.01	10	6613, 6607	2021
	100	2.01	10	6614, 6596	2021
	90	2.01	10	6615, 6597	2021
	80	2.01	10	6616, 6598	2021
	70	2.01	10	6617, 6599	2021
	60	2.01	10	6618, 6600	2021
	50	2.01	10	6619, 6601	2021
	40	2.01	10	6620, 6602	2021
	30	2.01	10	6621, 6603	2021
	20	2.01	10	6622, 6604	2021
	10	2.01	10	6623, 6605	2021
	5	2.01	10	6624, 6606	2021
Longitudinal field	5	1.96	0	4677, 4678	2022
	5	1.96	2.5	4679, 4680	2022
	5	1.96	5	4681, 4682	2022
	5	1.96	10	4683, 4684	2022
	5	1.96	125	4695, 4696	2022

Table 2: Low energy μSR run log for the $m = 1$ superlattice measured in zero, weak transverse, and longitudinal fields.

Measurement	T [K]	E [keV]	B [mT]	run no.	year
	275	2.01	0	4833	2021
	225	2.01	0	4832	2021
	150	2.01	0	4831	2021
Zero	75	2.01	0	4830	2021
field	37.5	2.01	0	4829	2021
	25	2.01	0	4828	2021
	17.5	2.01	0	4826	2021
	5	2.01	0	4827	2021
	300	2.01	10	4823	2021
	275	2.01	10	4822	2021
	250	2.01	10	4834	2021
	237	2.01	10	4821	2021
	225	2.01	10	4820	2021
	200	2.01	10	4819	2021
	175	2.01	10	4818	2021
	150	2.01	10	4817	2021
Weak	125	2.01	10	4816	2021
trans-	100	2.01	10	4815	2021
verse	75	2.01	10	4814	2021
field	50	2.01	10	4813	2021
	37.5	2.01	10	4824	2021
	31.27	2.01	10	4835	2021
	25	2.01	10	4812	2021
	21.3	2.01	10	4836	2021
	17.5	2.01	10	4825	2021
	14	2.01	10	4837	2021
	10	2.01	10	4810	2021
	5	2.01	10	4811	2021

Table 3: Low energy μSR run log for the $m = 2$ superlattice measured in zero and weak transverse fields.

Measurement	T [K]	E [keV]	B [mT]	run no.	year
Zero field	250	1.96	0	4158	2021
	200	1.96	0	4155	2021
	160	1.95	0	4156	2021
	120	1.95	0	4157	2021
	80	1.95	0	4152	2021
	50	1.96	0	4154	2021
	25	1.95	0	4153	2021
Weak transverse field	320	2.01	10	4140	2021
	300	2.01	10	4139	2021
	275	2.01	10	4138	2021
	250	2.01	10	4137	2021
	225	2.01	10	4136	2021
	200	2.01	10	4135	2021
	175	2.01	10	4134	2021
	170	2.01	10	4141	2021
	160	2.01	10	4142	2021
	150	2.01	10	4143,4133	2021
	140	2.01	10	4144	2021
	130	2.01	10	4145	2021
	125	2.01	10	4132	2021
	120	2.01	10	4146	2021
	110	2.01	10	4147	2021
	100	2.01	10	4131	2021
	75	2.01	10	4148	2021
	50	2.01	10	4149	2021
	25	2.01	10	4150	2021
	10	2.01	10	4151	2021

Table 4: Low energy μSR run log for the $m = 3$ superlattice measured in zero and weak transverse fields.

References

[1] Prokscha, T. et al. The new beam at psi: A hybrid-type large acceptance channel for the generation of a high intensity surface-muon beam. *Nucl. Instrum. Methods Phys. Res. A: Accel. Spectrom. Detect. Assoc. Equip.* **595**, 317–331 (2008). https://doi.org/10.1016/j.nima.2008.07.081

[2] Suter, A., Martins, M. M., Ni, X., Prokscha, T. & Salman, Z. Low energy measurements in Low-Energy μSR. *J. Phys.: Conf. Ser.* **2462**, 012011 (2023). https://doi.org/10.1088/1742-6596/2462/1/012011

[3] Eckstein, W. *Computer Simulation of Ion-Solid Interactions*, vol. 10 (Springer Berlin Heidelberg, 1991). https://doi.org/10.1007/978-3-642-73513-4

[4] Clark, L. et al. Gapless spin liquid ground state in the $S=1/2$ vanadium oxyfluoride kagome antiferromagnet $[NH_4]_2[\mathbf{C_7H_{14}N}][\mathbf{V_7O_6F_{18}}]$. *Phys. Rev. Lett.* **110**, 207208 (2013). https://doi.org/10.1103/PhysRevLett.110.207208

[5] Grutter, A. J. et al. Strain-induced competition between ferromagnetism and emergent antiferromagnetism in $(Eu,Sr)MnO_3$. *Phys. Rev. Mater.* **2**, 094402 (2018). https://doi.org/10.1103/PhysRevMaterials.2.094402

[6] Salman, Z. et al. Direct spectroscopic observation of a shallow hydrogen-like donor state in insulating $SrTiO_3$. *Phys. Rev. Lett.* **113**, 156801 (2014). https://doi.org/10.1103/PhysRevLett.113.156801

[7] Fowlie, J. et al. Intrinsic magnetism in superconducting infinite-layer nickelates. *Nat. Phys.* **18**, 1043–1047 (2022). https://doi.org/10.1038/s41567-022-01684-y

[8] Hayano, R. S. et al. Zero-and low-field spin relaxation studied by positive muons. *Phys. Rev. B* **20**, 850–859 (1979). https://doi.org/10.1103/PhysRevB.20.850

[9] Keren, A. Generalization of the abragam relaxation function to a longitudinal field. *Phys. Rev. B* **50**, 10039–10042 (1994). https://doi.org/10.1103/PhysRevB.50.10039

[10] Holzschuh, E., Denison, A. B., Kündig, W., Meier, P. F. & Patterson, B. D. Muon-spin-rotation experiments in orthoferrites. *Phys. Rev. B* **27**, 5294–5307 (1983). https://doi.org/10.1103/PhysRevB.27.5294